RSC Advances

PAPER

View Article Online
View Journal | View Issue

Check for updates

Cite this: *RSC Adv.*, 2022, **12**, 4550

Nitrogen-doped lignin-derived carbon for catalytic reduction of hexavalent chromium *via* HCOOH-mediated hydrogenation†

Yun Liu, *[ab] Haihua Yang[b] and Tao Chen[c]

It is highly desirable to explore efficient catalysts for reducing toxic Cr^{6+} to benign Cr^{3+} under mild and eco-friendly conditions. This article describes a facile fabrication of nitrogen doped carbon (N@C-g-C_3N_4) as a metal-free catalyst for Cr^{6+} reduction using lignin as a carbon source and g-C_3N_4 nanosheets as a nitrogen source. The structural properties of the N@C-g-C_3N_4 catalyst are characterized by TEM, HR-TEM, XRD, TGA, Raman, EDS-mapping, XPS and BET techniques. The summation of these analyses sheds light on the high surface area (903 $m^2\ g^{-1}$), mesopore size (17.3 nm) and defects (I_D/I_G = 0.97) of N@C-g-C_3N_4, which contribute to its excellent catalytic activity in HCOOH-mediated reduction of Cr^{6+} to Cr^{3+} with high rate constant (2.98 min^{-1}) and turnover frequency (2.21 $mol_{k2Cr2O7}\ g_{catalyst}^{-1}\ min^{-1}$) and complete degradation (100%) within 5 min. The catalytic performance of the catalyst reveals that the reduction activity is significantly dependent on the concentration of Cr^{6+} and HCOOH, catalyst loading, pH, temperature, and foreign ions. Particularly, the N@C-g-C_3N_4 catalyst shows superior stability and renewability with little loss of activity (≥95%) after 8 months storage and five repeated uses. Furthermore, N@C-g-C_3N_4 can be applied in other hydrogenation reactions involving $K_3[Fe(CN)_6]$, 4-NP and BPA using $NaBH_4$ as a hydrogen donor, and the removal of organic dyes. These findings illustrate that N@C-g-C_3N_4 as a metal-free catalyst is effective, versatile and eco-friendly for the reduction of Cr^{6+} from contaminated environments.

Received 24th August 2021
Accepted 22nd December 2021

DOI: 10.1039/d1ra06391j

rsc.li/rsc-advances

Open Access Article. Published on 04 February 2022. Downloaded on 5/3/2026 9:12:31 AM.
This article is licensed under a Creative Commons Attribution-NonCommercial 3.0 Unported Licence.

1 Introduction

Hexavalent chromium (Cr^{6+}) is commonly regarded as a very hazardous contaminant to humans and ecosystems because of carcinogenic and mutagenic issues.[1] It is indispensable to explore eco-friendly approaches for catalytic conversion of toxic Cr^{6+} into benign Cr^{3+} under mild and eco-friendly conditions, in which the core factor is the development of efficient catalysts.[2] Recently, supported noble metal (*e.g.*, Pd, Pt, Ag, and Au) catalysts have been extensively applied in the catalytic reduction of Cr^{6+} from aqueous environments.[3–5] For instance, Dai and co-workers investigated coenzyme A-regulated Pd nanocatalysts for HCOOH-mediated reduction of Cr^{6+} with the highest reduction rate of 2.45 mmol $mg^{-1}\ min^{-1}$ at 50 °C.[3] Celebi and co-workers synthesized Pd nanoparticles decorated on graphene oxide for Cr^{6+} reduction in the presence of HCOOH with the mass specific activity of 3.6 $mol_{K_2Cr_2O_7}\ mol_{Pd}^{-1}\ min^{-1}$ at room temperature.[6] Shao and co-workers described AuPd@Pd core–shell nanocrystals for HCOOH-mediated reduction of Cr^{6+} with a rate constant of up to 1.44 min^{-1}.[7] In comparison with noble metals, transition metal supported catalysts have already attracted tremendous interest owing to their low cost and abundant resources on earth.[8,9] As an example, Xu and co-workers prepared cobalt nanoparticles supported on reduced graphene oxide (Co–RGO) for Cr^{6+} reduction in the presence of HCOOH with mass specific activity value of 0.049 $mol_{K_2Cr_2O_7}\ mol_{Co}^{-1}\ min^{-1}$ at room temperature.[8] In another study, Bhowmik and coworkers developed nickel nanoparticles supported on reduced graphene oxide (Ni–RGO) for Cr^{6+} reduction with the mass specific activity value of 0.014 $mol_{K_2Cr_2O_7}\ mol_{Ni}^{-1}\ min^{-1}$.[9] In 2021, Nie and co-workers summarized transition metal based catalysts for transfer hydrogenation with HCOOH as hydrogen donor through transfer hydrogenation, hydrogenolysis, and hydrodechlorination reactions.[10] Different from molecular hydrogen (H_2), formic acid (FA, HCOOH) has emerged as a green and renewable hydrogen donor which requires no elaborate experimental setups and can avoid substrate over-reduction.[10]

However, the above-mentioned noble and/or non-noble metals supported catalysts always result in cost and environmental issues, therefore, metal-free catalysts, such as various carbon based materials, should be explored as low-cost and benign heterogeneous catalysts in this field. These carbon-

[a]*Hubei Key Laboratory of Radiation Chemistry and Functional Materials, Hubei University of Science and Technology, Xianning 437100, China*

[b]*Beijing Key Laboratory of Bioprocess, College of Life Science and Technology, Beijing University of Chemical Technology, Beijing 100029, China. E-mail: liuyunprivate@sina.com; liuyun@mail.buct.edu.cn; Fax: +86-010-64416428; Tel: +86-010-64421335*

[c]*School of Nuclear Technology and Chemistry & Biology, Hubei University of Science and Technology, Xianning 437100, China*

† Electronic supplementary information (ESI) available. Fig. S1–S15 and Tables S1 and S2. See DOI: 10.1039/d1ra06391j

© 2022 The Author(s). Published by the Royal Society of Chemistry

Open Access Article. Published on 04 February 2022. Downloaded on 5/3/2026 9:12:31 AM. This article is licensed under a Creative Commons Attribution-NonCommercial 3.0 Unported Licence.

based metal-free catalysts have been used for oxygen reduction reaction (ORR), oxygen evolution reaction (OER), hydrogen evolution reaction (HER) and 4-nitrophenol reduction so far.[11–13] It is generally considered that heteroatom dopants (N, P, S, B, *etc.*) can improve the catalytic performance of carbon materials by changing the electronic structure of adjacent carbon and/or producing additional active sites.[14] These carbon-based materials used as metal-free heterogeneous catalysts have been widely conducted in organic synthesis and electrochemical fields.[14,15] However, up to date, little information has been available on the reduction of Cr^{6+} by nitrogen-doped carbon through transfer hydrogenation in the presence of HCOOH in literature.

The objectives of the present work are to fabricate an efficient nitrogen-doped carbon as metal-free catalyst for Cr^{6+} reduction and to investigate the effect of the nitrogen source (g-C_3N_4, urea, dicyandiamide, melamine) and annealing temperature (650 °C, 750 °C, 850 °C, 950 °C) on the reduction of Cr^{6+} by nitrogen-doped carbon *via* HCOOH-mediated hydrogenation. As an example, a novel nitrogen-doped carbon (N@C-g-C_3N_4) catalyst was successfully fabricated through lignin/Zn^{2+} coordination coating on g-C_3N_4 nanosheets followed by calcination in argon atmosphere. The role of Zn^{2+} addition was used as a pore-forming chemical, which is always introduced in the pyrolysis process to yield high surface area and hierarchical porous carbon.[16] Lignin chosen as carbon source is the fact that lignin is a byproduct of pulp and papermaking, which accounts for 2.5×10^7 tons of lignin produced each year. The development of lignins for high value carbon materials has the potential for a high payoff for biomass biorefinery. g-C_3N_4 nanosheets chosen as nitrogen source is contributed to its high surface specific area and nitrogen content (approx. 52%).[13] The as-synthesized N@C-g-C_3N_4 was characterized by TEM, HR-TEM, TGA, Raman, EDS-mapping, XPS and BET analysis. The as-obtained N@C-g-C_3N_4 exhibits excellent catalytic activity in the HCOOH-mediated reduction of toxic Cr^{6+} to benign Cr^{3+}. The reduction efficiency is significantly dependent on the concentration of Cr^{6+} and HCOOH, catalyst loading, pH, temperature, and foreign ions. The catalytic mechanism of Cr^{6+} reduction over N@C-g-C_3N_4 in the presence of HCOOH is different from that using molecular hydrogen as reductant. It is worthily noticed that N@C-g-C_3N_4 catalyst shows superior stability and renewability with little loss of activity after 8 months storage and five repeated usage. In addition, the N@C-g-C_3N_4 catalyst shows satisfactory adsorption activities in the removal of organic dyes including methyl red, methyl blue, methylene blue (MB), and congo red. It also possesses efficiently catalytic performance for hydrogenation reactions involving $K_3[Fe(CN)_6]$, 4-nitrophenol (4-NP) and bisphenol A (BPA) reduction using $NaBH_4$ as hydrogen donor. It is indisputable that the N@C-g-C_3N_4 is an effective and versatile viable catalyst for the reduction of Cr^{6+} and other toxic organic dyes from wastewater.

2 Material and methods

2.1 Materials

All the chemicals including lignin, formic acid (HCOOH), urea, dicyandiamide (DCA), melamine, 4-nitrophenol (4-NP), bisphenol A (BPA), methyl red, methyl blue, methylene blue (MB), congo red, and phenolphthalein were all of high purity and commercially available from Aladdin, Shanghai, China. Other chemicals such as zinc acetate ($Zn(OAc)_2$), potassium ferrocyanide trihydrate ($K_3[Fe(CN)_6]$), potassium dichromate ($K_2Cr_2O_7$), sodium hydroxide (NaOH) were purchased from Beijing Chemical Regent Company, China.

2.2 Catalyst synthesis

2.2.1 Synthesis of g-C_3N_4 nanosheets. g-C_3N_4 nanosheets were produced from urea through duplicate annealing at 550 °C in a muffle furnace according to the modified procedures reported in our previous work.[13] Typically, 10 g of urea was put in a crucible with a cover, and heated at 550 °C in a muffle furnace with the temperature rate of 2 °C min^{-1} for 4 h. The resultant yellow powder was further thermally exfoliated at 550 °C in a muffle furnace with the temperature rate of 5 °C min^{-1} for 2 h. Subsequently, the g-C_3N_4 nanosheets were obtained with the final yield of approx. 4.5%. The N content in g-C_3N_4 was detected to be approx. 52% by element analyzer.

2.2.2 Fabrication of nitrogen-doped carbon (N@C) catalyst. Typically, 3.5 g of lignin was dissolved in 300 mL deionized water under mechanical stirring condition, and then 50 mL of $Zn(OAc)_2 \cdot 2H_2O$ (14 mmol Zn^{2+}, acting as pore-forming chemical) solution were added into lignin solution and kept continuous stirring at 800 rpm for 2 h. Subsequently, 10.5 g of the as-synthesized g-C_3N_4 nanosheets as soft template was slowly put into the mixture solution and ultrasonic dispersion for 30 min. Afterwards, the mixture solution was continued to stir at 800 rpm for another 2 h and kept it at room temperature for overnight aging. Through centrifugation, the g-C_3N_4 nanosheets coated with lignin/Zn^{2+} coordination (g-C_3N_4@lignin/Zn^{2+}) were collected and washed with deionized water for three times and dried at 80 °C for 5 h. The resultant g-C_3N_4@lignin/Zn^{2+} composites were annealed in a tube furnace at 550 °C for 2 h, and then at fixed temperature (650 °C, 750 °C, 850 °C and 950 °C) for another 4 h under an argon atmosphere with the flow rate of 50 mL min^{-1}. After cooling to room temperature, the nitrogen doped carbon using g-C_3N_4 as nitrogen dopant (N@C-g-C_3N_4) was obtained. For clarity, N@C-g-C_3N_4-*T* refers to samples prepared at annealing temperature of *T* °C. To examine the influence of different nitrogen sources, several other counterparts of nitrogen-doped carbon were also fabricated using a similar procedure, but melamine (mela), dicyandiamide (DCA), and urea as nitrogen dopant in place of g-C_3N_4. These resultant samples were denoted as N@C-mela-*T*, N@C-DCA-*T*, and N@C-urea-*T*, respectively. As control, lignin with Zn^{2+} pore-forming chemical was calcined under the same conditions to achieve lignin-derived carbon (LC) in the absence of nitrogen dopant.[16]

2.3 Catalyst characterization

X-ray diffraction (XRD) was recorded on a Rigaku Ultima IV diffractometer at 30 kV using Cu Kα radiation (λ = 1.54, 10° min^{-1} from 3 to 90°). X-ray photoelectron spectroscopy (XPS) was performed on a ThermoFisher Scientific ESCALAB

Open Access Article. Published on 04 February 2022. Downloaded on 5/3/2026 9:12:31 AM. This article is licensed under a Creative Commons Attribution-NonCommercial 3.0 Unported Licence.

250XI using monochromated Al Kalph source (150 W, 500 μm). TEM images with EDX mapping were collected on a JEM-F200 equipped with an energy dispersive X-ray (EDX) spectroscopy at 10 kV. Raman spectra were conducted on a Horiba HR evolution Raman spectroscopy system at 532 nm and 12.5 mA laser powder. Thermogravity analysis (TGA) was performed on a PerkinElmer STA 8000 thermoanalyzer under flowing nitrogen at 50 mL min^{-1}, the temperature was ranged from 100 to 1000 °C at the heating rate of 10 °C min^{-1}. Brunauer–Emmett–Teller (BET) analyses were performed on Micromeritics ASAP 2460 using N_2. The samples were degassed at 250 °C for 12 h before measurement. Atom force microspectroscopy (AFM) was conducted on a Bruker Nanoscope.

2.4 Catalytic reduction activity of catalyst

Typically, 25 mg of the as-prepared N@C catalyst was added into the mixture solution containing 25 mL $K_2Cr_2O_7$ (0.68 mM) and 1 mL HCOOH (98%) at room temperature under vigorously magnetic stirring. At a desired time interval, 200 μL of the reactants was drawn from the reaction system, and then diluted to 3 mL, and immediately monitored by UV756CRT UV-vis spectrophotometer (250–550 nm). Simultaneously, the color changes of reactants were also photographed using a digital camera. Furthermore, experiments on parameter optimum were carried out by changing the pH, HCOOH amount, catalyst loading, K_2CrO_7 concentration, reaction temperature and annealing temperature.

The apparent rate constant (k) was calculated from the plots of $\ln(C_t/C_0)$ *vs.* reaction time (t) in the following equation.

$$-k \times t = \ln \frac{C_t}{C_0} \quad \text{(I)}$$

where, C_0 and C_t stand for the concentration of Cr^{6+} in the system at the starting and reaction time, t, respectively.

The reaction activation energy (E_a) was calculated from Arrhenius equation as follows.

$$\ln\ k = \frac{-E_a}{RT} + \ln\ A \quad \text{(II)}$$

where, k is the apparent rate constant at designed reaction temperature, min^{-1}; A is the pre-exponential factor or Arrhenius constant, min^{-1}; E_a is the activation energy, kJ mol^{-1}; R is mole gas constant, 8.314 J mol^{-1} K^{-1}; T is the absolute temperature, K.

The mass specific activity of catalyst is calculated to the following equation

$$\text{Mass specific activity} = \frac{\Delta M_{K_2Cr_2O_7}}{w \times \Delta t} \quad \text{(III)}$$

where, $\Delta M_{K_2Cr_2O_7}$ is the concentration change of $K_2Cr_2O_7$ between starting and ending reaction, mmol; w is the weight of catalyst loading, mg; Δt is the reaction time change between starting and ending reaction, min.

Recycling experiments were conducted to evaluate the catalytic stability of N@C-g-C_3N_4-950 in the reduction of Cr^{6+} *via* HCOOH hydrogenation. After reaction, the catalyst was collected through filtration for the next batch reduction of Cr^{6+} under the same conditions of initial experiment. Simultaneously, N@C-g-C_3N_4-950 stored at room temperature for 8 months was investigated to assess its storage stability.

2.5 Comparative study using molecular hydrogen as a reductant

To explore the different catalytic mechanism using HCOOH and molecular hydrogen as reductant, a comparative study was designed to elucidate the role of hydrogen as a reductant in our work. The experimental set-up includes a balloon filled with hydrogen gas and an attached needle that allows free gas flow was directed into a three-neck reaction vessel.[4] The reduction of Cr^{6+} using elemental hydrogen was tested in a continuous gas flow into the reaction vessel containing 25 mL Cr^{6+} solution (0.68 mM) and 1 mL HCOOH (98%) with or without N@C-g-C_3N_4 catalyst (25 mg). Reaction temperature was fixed at 50 °C.

2.6 Determination of Cr^{6+} concentration and detection of Cr^{3+}

The variance of Cr^{6+} concentration was quantitatively measured on a UV756CRT UV-vis spectrophotometer by observing the intensity changes of the absorption peak of Cr^{6+} at 350 nm wavelength (the characteristic absorption peak for Cr^{6+}).[4] In the Cr^{6+} to Cr^{3+} conversion system in the presence of catalyst and HCOOH, Cr^{3+} as the reaction product was confirmed by adding sodium hydroxide solution. An excess of sodium hydroxide solution was added to a solution of hexaaquachromium(III) ions, a green solution of hexahydroxochromate(III) ions was produced demonstrating the presence of Cr^{3+}.[4]

2.7 Detection of CO_2 and H_2 from HCOOH decomposition

The total gas evolution was observed using vertical drainage method.[17] H_2 evolution from HCOOH was detected using GC-7900 gas chromatography equipped with thermal conductivity detector (TCD). The conditions of GC were: N_2 as carried gas, electric current 80 mA, column temperature 80 °C, injection temperature 120 °C, detection temperature 150 °C. CO_2 evolution from HCOOH was monitored by phenolphthalein in coloration method.

3 Results and discussion

3.1 Synthesis and characterization of catalysts

As an example, the schematic flow of N@C-g-C_3N_4 catalyst fabrication is illustrated in Fig. 1a. This procedure includes two steps: preparation of g-C_3N_4 nanosheet template and carbonization of g-C_3N_4 decorated with lignin/Zn^{2+} coordination. Specifically, g-C_3N_4 nanosheets were first prepared through duplicate thermal decomposition of urea (Fig. S1†). Subsequently, the lignin/Zn^{2+} coordination complexes were coated on the surface of g-C_3N_4 nanosheets. Finally, g-C_3N_4@ lignin/Zn^{2+} nanosheets were calcined at desired temperature in Ar atmosphere, leading to pyrolysis of g-C_3N_4 nanosheets and Zn^{2+} ions vaporation over 950 °C, and simultaneously carbonization of lignin. According to this procedure, nitrogen doped carbon (N@C) with different nitrogen dopant and calcination

 © 2022 The Author(s). Published by the Royal Society of Chemistry

Open Access Article. Published on 04 February 2022. Downloaded on 5/3/2026 9:12:31 AM.
This article is licensed under a Creative Commons Attribution-NonCommercial 3.0 Unported Licence.

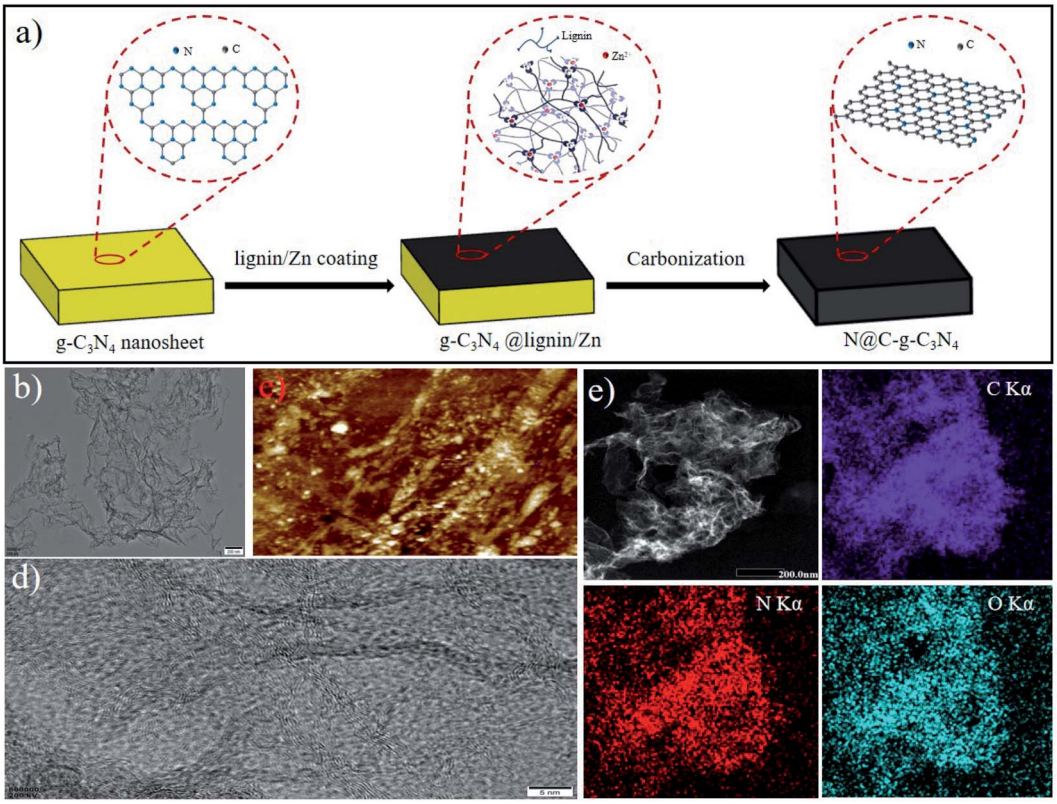

Fig. 1 Schematic illustration for preparing nitrogen doped carbon and characterization using N@C-g-C_3N_4 as an example. (a) Synthesis procedure; (b) TEM image; (c) AFM image; (d) HR-TEM image; (e) EDS-mapping analysis.

temperatures was obtained and labeled as N@C-X-*T*, X represents the nitrogen source and *T* stands for the annealing temperature (°C).

TEM image of N@C-g-C_3N_4-950 with wrinkle silk-like structure is shown in Fig. 1b, indicating the ultrathin feature of nanosheets. Representative AFM image in Fig. 1c shows that the light white dot on the surface of N@C-g-C_3N_4-950 is a bit thicker than other places, suggesting the thickness layer is not uniform and stacking (Fig. S2†). It is further confirming the wrinkle structure of N@C-g-C_3N_4-950 observed from TEM image. Due to the stacking and wrinkles of nanosheets, it was hard to accurately measure the thickness difference of carbon nanosheets. The interlayer distance of 0.34 nm corresponding to the (002) plane of graphite is confirmed by HR-TEM observation (Fig. 1d), it reveals the graphitic nature of the sample. Raman spectrum of N@C-g-C_3N_4-950 (Fig. S3†) shows two peaks at 1350 and 1590 nm, assigned to disordered sp^3 carbon (D band) and graphitic sp^2 carbon (G band), respectively.[14] The I_D/I_G intensity ratio is 0.97, confirming graphene character. Fig. S4† shows XRD pattern of N@C-g-C_3N_4-950 and g-C_3N_4 template. A narrow sharp peak at $2\theta = 23.6°$ of g-C_3N_4 is observed, whilst N@C-g-C_3N_4-950 shows a broad peak at $2\theta = 24.1°$, corresponding to (002) planes of graphite, suggesting the complete decomposition of g-C_3N_4 during annealing. It is further confirmed by TGA/DSC analyses of N@C-g-C_3N_4-950 with the weight loss of below 10% at 900 °C (Fig. S5†). STEM-EDS mapping of N@C-g-C_3N_4-950 reveals the homogeneous distribution of N atoms throughout the carbon nanosheets (Fig. 1e), indicating that the N atoms were simultaneously doped on the surface of carbon during thermal calcination. The N atom content of the sample is approx. 4.96 at%, which is similar with the value (4.84 at%) determined by XPS. The morphology of N@C-g-C_3N_4-950, lignin/Zn^{2+} coordination (LC carbon) and g-C_3N_4 was observed by SEM images. As observation from Fig. S6,† the morphology of g-C_3N_4 is like lamella structure, and LC carbon displays smooth bulk appearance. When lignin/Zn^{2+} coordination was coating on the surface of g-C_3N_4, N@C-g-C_3N_4-950 also show the same lamella morphology as g-C_3N_4. To confirm whether there exists Zn species in the catalyst, ICP-OES examination was conducted and no Zn content was detected.

XPS analysis was carried out to characterize the nitrogen species in the N@C catalyst samples. The results are summarized in Fig. 2 and Table S1.†

As seen from Fig. 2 and Table S1,† the XPS survey spectrum confirms that nitrogen source shows significant effect on the N content in N@C samples. Specifically, the contents of N element in N@C-g-C_3N_4-950, N@C-mela-950, N@C-DCA-950 and N@C-urea-950 are 4.84 at%, 3.90 at%, 3.98 at% and 2.76 at%, respectively. It indicates that g-C_3N_4 nanosheet is promising N dopant source for N@C catalyst synthesis.[13] Similarily, the N content can be easily controlled by the carbonization temperature. Samples of N@C-g-C_3N_4 after calcined at 650 °C, 750 °C, and 850 °C were prepared and the N contents in N@C-g-C_3N_4-650, N@C-g-C_3N_4-750, and N@C-g-C_3N_4-850 are 18.37 at%,

© 2022 The Author(s). Published by the Royal Society of Chemistry

Open Access Article. Published on 04 February 2022. Downloaded on 5/3/2026 9:12:31 AM.
This article is licensed under a Creative Commons Attribution-NonCommercial 3.0 Unported Licence.

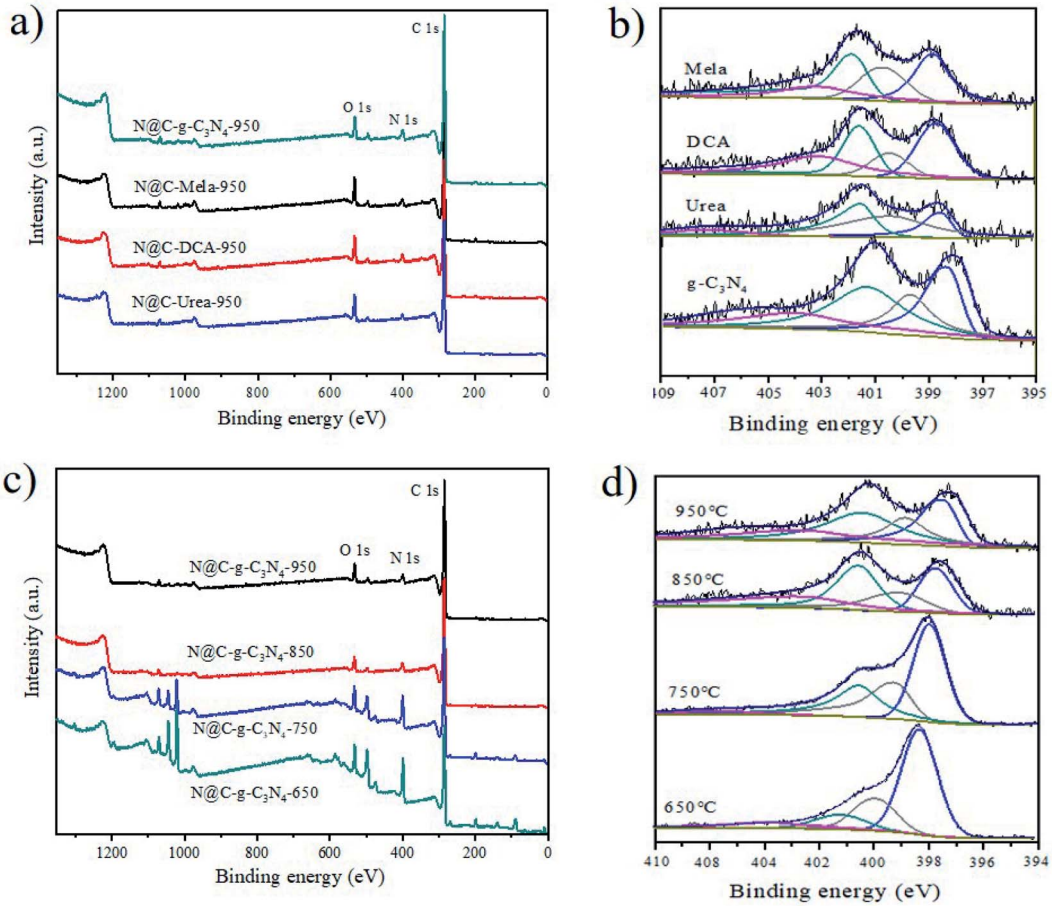

Fig. 2 XPS spectra of N@C samples with different nitrogen dopants and annealing temperature. (a) XPS survey of N@C samples with different nitrogen dopants; (b) N1s spectra of N@C samples with different nitrogen dopants; (c) XPS survey of N@C-g-C_3N_4 at different annealing temperatures; (d) N1s spectra of N@C-g-C_3N_4 at different annealing temperatures.

13.43 at% and 6.68 at%, respectively (Table S1 and Fig. S7†). As shown in Table S1,† the carbon element content increases while the contents of oxygen and nitrogen elements decrease with increasing carbonization temperature. As shown from the high-resolution N1s spectra of N@C samples in Fig. 2b and d, it can be divided into four peaks at 398.6 eV (pyridinic N), 400.5 eV (pyrodic N) 401.1 eV (graphitic N) and 403.5 eV (oxidization N) with ratios of 9.70%, 19.40%, 54.73% and 16.17%, respectively.[18] It is worthily to notice that the ratios of N species are significantly dependent on N sources and calcination temperature. As seen in Table S2 and Fig. S8,† the contents of N species are obviously different, and graphitic N became dominant with increasing calcination temperature. The relative ratio of graphitic N in N@C-g-C_3N_4-950 was the highest (54.73 at%) among all samples. Higher content of graphitic N, higher catalytic activity of N@C catalyst exhibits.[13]

BET surface area and pore diameter of the N@C samples play a vital role in the catalytic performance. The N_2 adsorption–desorption isotherms of the as-obtained N@C samples are tested and BET profiles are shown in Fig. 3. It is observed that all samples except from N@C-urea-950 appear in their hysteresis loops, showing the typical-IV curve, it is demonstrated the existence of both micro- and meso-pores. As seen from Fig. 3a–d, the BET specific surface areas of N@C-g-C_3N_4-950, N@C-mela-950, N@C-DCA-950 and N@C-urea-950 are 903, 213, 602 and 633 $m^2\ g^{-1}$, respectively. The highest surface area of N@C-g-C_3N_4-950 is likely relate to the high graphitization degree, ultrathin g-C_3N_4 nanosheet template and multiporous property. Noticeably, calcination temperature has a great impact on the BET specific areas of N@C-g-C_3N_4. The BET specific surface areas of N@C-g-C_3N_4-650, N@C-g-C_3N_4-750, N@C-g-C_3N_4-850 and N@C-g-C_3N_4-950 are 362, 570, 870 and 903 $m^2\ g^{-1}$, respectively. The released gases during the thermal decomposition of g-C_3N_4 nanosheets introduce additional mesopores, and thus enhance the surface area of carbon nanosheets. Furthermore, different nitrogen sources also show a significant influence on the BET specific areas of N@C samples. More detail information on specific surface area and pore size of all samples are summarized in Table S1.†

3.2 Catalytic reduction of Cr^{6+} over N@C catalysts *via* HCOOH-mediated hydrogenation

The catalytic activities of N@C catalysts were tested by employing HCOOH-mediated reduction of much harmful Cr^{6+}

© 2022 The Author(s). Published by the Royal Society of Chemistry

Open Access Article. Published on 04 February 2022. Downloaded on 5/3/2026 9:12:31 AM.
This article is licensed under a Creative Commons Attribution-NonCommercial 3.0 Unported Licence.

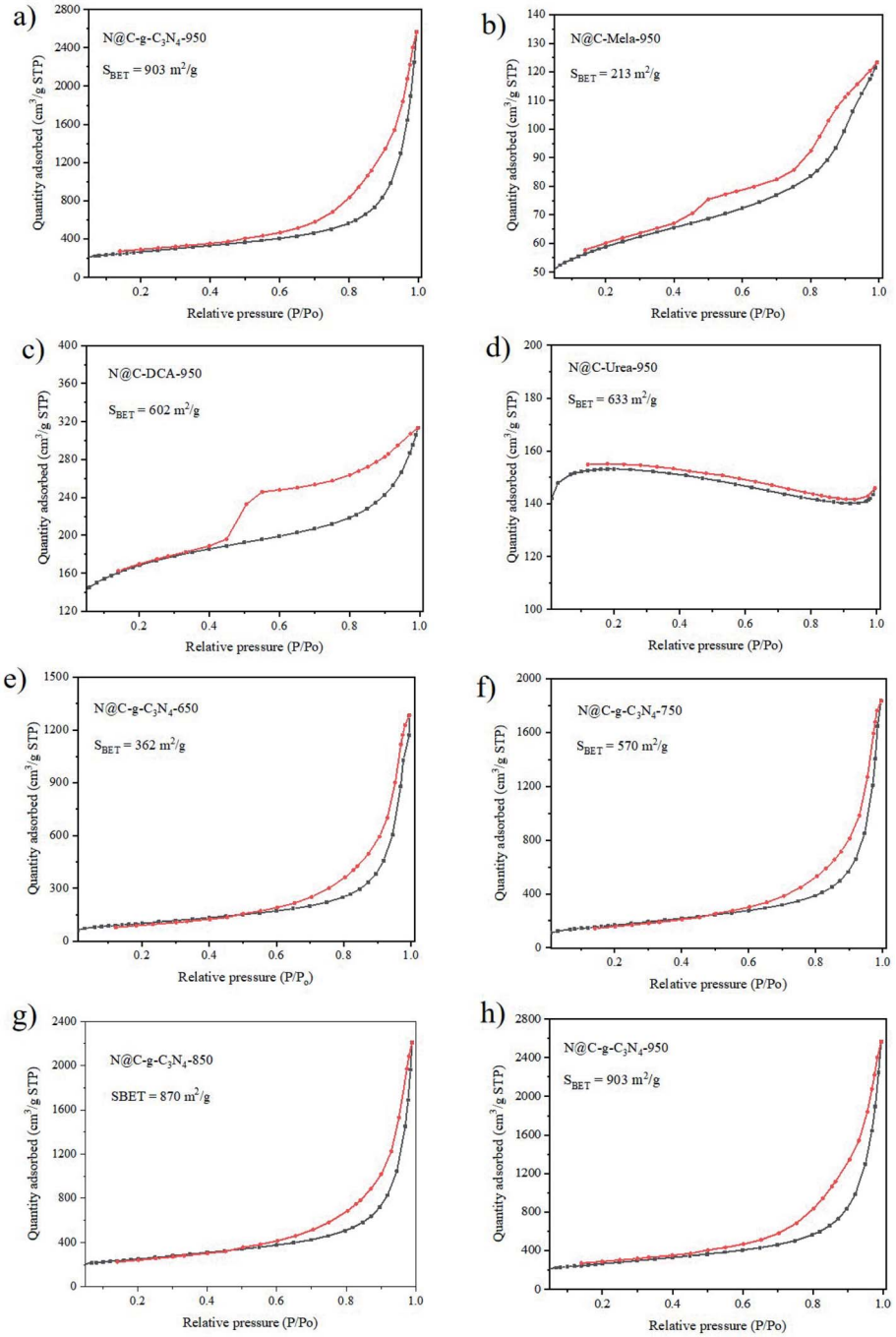

Fig. 3 BET surface area analyses of N@C with different N sources at 950 °C (a–d) and BET surface area of N@C-g-C_3N_4 at different annealing temperatures ranging from 650 to 950 °C (e–h).

to benign Cr^{3+} at room temperature. $K_2Cr_2O_7$ was chosen as one of the representatives of Cr^{6+} in this work. The reduction process of Cr^{6+} was monitored at 350 nm on a UV-vis spectroscopy.[1] As shown in Fig. 4a, it is worthily noticed that N@C-g-C_3N_4 shows excellent performance toward the HCOOH-assisted catalytic reduction of Cr^{6+} to Cr^{3+}. While both LC carbon and g-C_3N_4 materials display negligible catalytic activity of Cr^{6+} reduction. For comparison, Cr^{6+} is not reduced by N@C-g-C_3N_4 catalyst alone or HCOOH-treatment without addition of catalyst. It indicates that the catalytic reduction of Cr^{6+} to Cr^{3+} is initiated by both catalyst and HCOOH, in other words, N@C-g-C_3N_4 catalyst and HCOOH as hydrogen donor are the two core factors for the catalytic reduction of Cr^{6+} to Cr^{3+} from aqueous environment.

As seen from Fig. 4b, effect of different nitrogen source in N@C catalysts is significant on HCOOH-mediated reduction of Cr^{6+}. The catalytic activities of catalysts decrease with the order of N@C-g-C_3N_4-950 > N@C-DCA-950 > N@C-mela-950 > N@C-

Open Access Article. Published on 04 February 2022. Downloaded on 5/3/2026 9:12:31 AM.
This article is licensed under a Creative Commons Attribution-NonCommercial 3.0 Unported Licence.

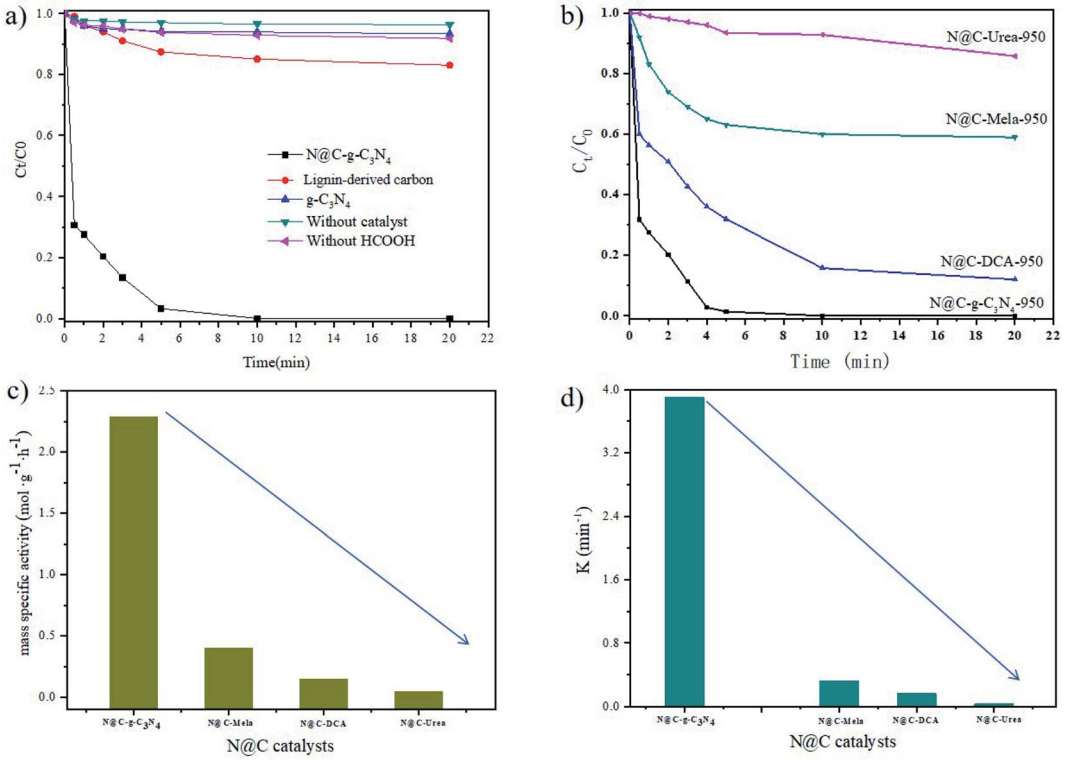

Fig. 4 Comparison of catalytic performance for Cr^{6+} reduction by different N@C catalysts in the presence of HCOOH. (a) effects of N@g-C_3N_4 catalyst in presence of HCOOH; (b) effects of different nitrogen source; (c) mass specific activity of N@C catalysts with different N source; (d) rate constant (k) values N@C catalysts with different N source. Reaction conditions: 25 mL $K_2Cr_2O_7$ (0.68 mM), 1 mL HCOOH (98%), 25 mg catalyst, temperature 50 °C, stirring rate 500 rpm.

urea-950. These results are further confirmed in Fig. S9† by the absorbance decrease *vs.* time plots towards the catalytic reduction of Cr^{6+}. It is observed that the reduction time of Cr^{6+} by N@C-DCA, N@C-mela, and N@C-urea is much longer than N@C-g-C_3N_4. The absorption intensity at 350 nm rapidly decreases upon addition of N@C-g-C_3N_4 within 5 min, accompanied by a color change of yellow to colorless (Fig. S10†), indicating the effective reduction of Cr^{6+}. The obtained colorless solution immediately becomes green color by adding excess NaOH solution, which demonstrates the formation of Cr^{3+} complex ($[Cr(OH)_6]^{3-}$) (Fig. S10†). From the observation of mass specific activity values in Fig. 4c and k values in Fig. 4d, it is further demonstrated that N@C-g-C_3N_4 shows the best catalytic performance toward the HCOOH-mediated reduction of toxic Cr^{6+} to benign Cr^{3+} among all prepared N@C catalysts (Fig. S11†). The high catalytic efficiency of N@C-g-C_3N_4 is contributed to the combination effects of its high S_{BET}, mesoporous size structure and N species (Table S1, Fig. S7 and S8†). It is observed in Fig. 4c that the mass specific activity value of N@C-g-C_3N_4 (2.21 mol $_{K_2Cr_2O_7}$ g^{-1} min^{-1} at 323 K) is the highest among all samples, which is superior to the previously reported Pd-based catalysts (0.02–1.43 $mol_{K_2Cr_2O_7}$ g_{Pd}^{-1} min^{-1}) in literatures.[18–21] As seen in Fig. 4d, the highest k value was calculated to be 2.98 min^{-1} for N@C-g-C_3N_4 at 50 °C, higher than that of CoA–Pd heterogeneous catalyst (k = 0.602 min^{-1}) reported in literature.[3]

The critical parameters impacting the catalytic performance of N@C-g-C_3N_4 for HCOOH-mediated reduction of Cr^{6+} include pH, HCOOH amount, catalyst loading, reaction temperature, and $K_2Cr_2O_7$ concentration. To investigate the effect of HCOOH concentration on catalytic performance, the other parameters are keeping stable as follows: 25 mL $K_2Cr_2O_7$ (0.68 mM), 25 mg catalyst, temperature 50 °C, and stirring rate 500 rpm. The data in Fig. 5a further reveal that for 0.4 to 1.0 mL additions of 98% HCOOH, an increase of the catalytic reduction of Cr^{6+} is observed, indicating that the availability of a catalyst active surface area is enough for HCOOH decomposition.[1,2] However, there is no positive outcome with further additional rise in HCOOH concentration from 1.0 to 1.3 mL due to the excess of HCOOH without decomposition. It is therefore demonstrated that 1.0 mL addition of HCOOH is suitable for the catalytic reduction of Cr^{6+}. The more of the obtainability of additional active surface area for HCOOH decomposition, the better of the reduction of Cr^{6+}.[1] Fig. S12† shows that Cr^{6+} is almost completely reduced by N@C-g-C_3N_4 within 5 minutes when HCOOH concentration ranges from 0.01 mM to 0.04 mM by keeping other parameters constant. When other parameters are keeping stable as follows: 25 mL $K_2Cr_2O_7$ (0.68 mM), 1 mL HCOOH (98%), temperature 50 °C, and stirring rate 500 rpm, the effect of catalyst loading on performance are shown in Fig. 5b. As seen in Fig. 5b, the increase in efficiency of the reduction Cr^{6+} is obtained by increasing the N@C-g-C_3N_4

© 2022 The Author(s). Published by the Royal Society of Chemistry

Open Access Article. Published on 04 February 2022. Downloaded on 5/3/2026 9:12:31 AM.
This article is licensed under a Creative Commons Attribution-NonCommercial 3.0 Unported Licence.

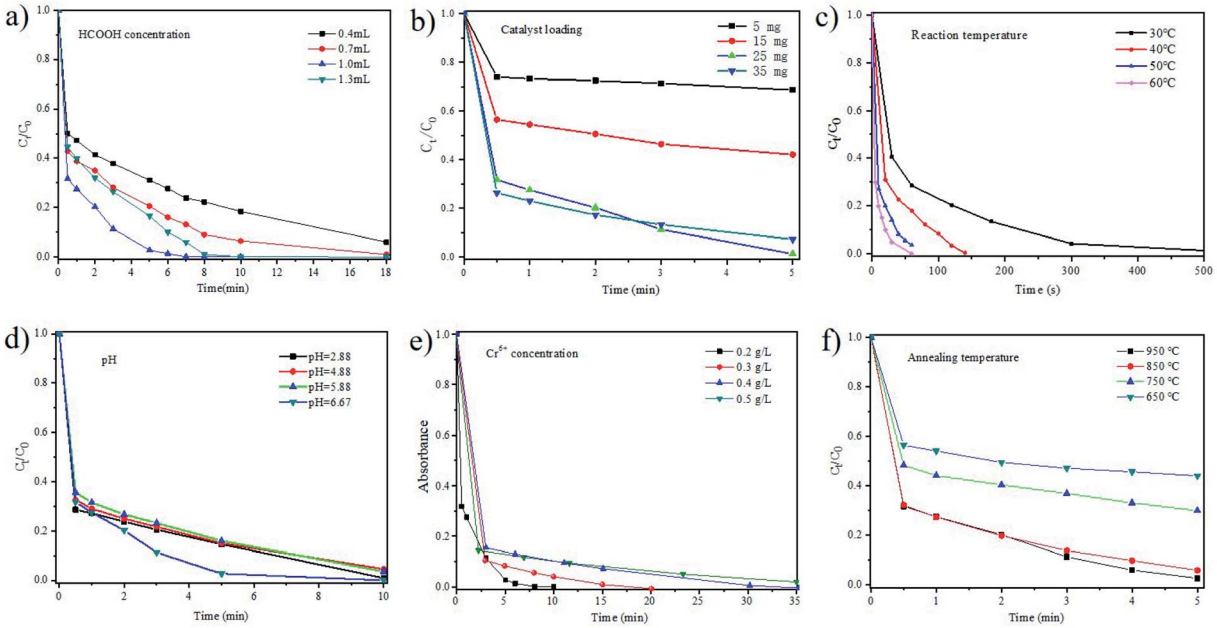

Fig. 5 Parameters optimization the catalytic performance of N@C-g-C_3N_4 for HCOOH-mediated reduction of Cr^{6+}. (a) HCOOH concentration; (b) catalyst loading; (c) reaction temperature; (d) pH; (e) Cr^{6+} concentration; (f) annealing temperature.

catalyst loading from 5 mg to 35 mg due to more active site in case of higher catalyst loading. However, the rate variation with further mass loading shows no change between 25 and 35 mg. It seems that this may be at the diffusion limit. It was reported, for metal-based catalyst, that there existed the decrease in total surface area or aggregation of particles at a high concentration of catalyst.[22] The effect of reaction temperature on Cr^{6+} catalytic reduction was investigated from 30 °C to 60 °C (Fig. 5c and S13†). When other parameters are keeping constant as follows: 25 mL $K_2Cr_2O_7$ (0.68 mM), 1 mL HCOOH (98%), 25 mg catalyst, and stirring rate 500 rpm, the catalytic reduction efficiency increases with the rise of the reaction temperature (Fig. 5c), due to increasing the availability of active surface area of the catalyst for HCOOH decomposition.[2] The catalytic efficiency of N@C-g-C_3N_4 is very well concision with that of Pd/Ag alloy reported in literature.[17,23–25] It is inevitable that the influence of initial pH on the catalytic reduction of Cr^{6+}. As shown in Fig. 4d, a higher rate of catalytic reduction is observed at low pH value (pH < 6.0) when the conditions are conducted under the conditions of 25 mL $K_2Cr_2O_7$ (0.68 mM), 1 mL HCOOH (98%), 25 mg catalyst, temperature 50 °C, and stirring rate 500 rpm, and this result is considerably confirmed by the previously reported articles.[2,4] Vellaichamy and co-workers reported that the catalytic reduction efficiency decreased at basic conditions, the reasonable explanation was the fact that reduction product, Cr^{3+}, forms $Cr(OH)_3$ precipitate over the surface of the catalysts.[1] When other parameters are keeping constant as follows: 1 mL HCOOH (98%), 25 mg catalyst, temperature 30 °C, stirring rate 500 rpm, the impact of Cr^{6+} concentration on its catalytic reduction was carried out and the results are shown in Fig. 4e. Decrease in the catalytic reduction performance is observed with the increase of the initial Cr^{6+} concentration from 0.2 g L^{-1} to 0.5 g L^{-1}. The reasonable explanation is the fact that the higher concentration of Cr^{6+} will hinder the active surface of the catalyst or even block the catalyst *via* screening or shielding effects. This kind of shielding of Cr^{6+} species makes it more difficult for HCOOH decomposition, thereby lowering the conversion rate of Cr^{6+} to Cr^{3+}.[1,26] As shown in Fig. 5f, different annealing temperature of catalyst preparation shows significant effect on the its catalytic reduction efficiency of Cr^{6+}, because higher specific surface area of catalyst is obtained at higher annealing temperature (Fig. 3). High specific surface area of catalyst is helpful for absorption of HCOOH and Cr^{6+} to increase catalytic reduction activity.

3.3 Mechanism of HCOOH-mediated reduction of Cr^{6+} by N@C-g-C_3N_4 catalyst

To throw light on the catalytic mechanism of HCOOH-mediated reduction of Cr^{6+} by N@C-g-C_3N_4 catalyst, a comparative study was conducted using molecular hydrogen (H_2) as reductant. As shown in Fig. 6a, absorbance at 350 nm only slightly decreases even prolonging reaction time to 60 min when hydrogen is used as reductant in the absence of catalyst, and less than 10% of Cr^{6+} is reduced to Cr^{3+} (Fig. 6b). Subsequently, use of hydrogen as reductant in the presence of N@C-g-C_3N_4 can obtain absorbance intensity decrease within 5 min at 350 nm (Fig. 6a), and approx. 48% of the initial Cr^{6+} is converted into Cr^{3+} (Fig. 6b). On the contrary, HCOOH-mediated reduction in the presence of N@C-g-C_3N_4 can achieve nearly 100% complete reduction of Cr^{6+} within 5 min, much higher than that using molecular hydrogen (H_2) as reductant (Fig. 6b). These comparison results confirm that there exist different catalytic mechanism between H_2-mediated and HCOOH-mediated reduction of Cr^{6+} in the presence of catalyst. To date, a common consensus is widely accepted that the chemical decomposition of HCOOH is

Open Access Article. Published on 04 February 2022. Downloaded on 5/3/2026 9:12:31 AM.
This article is licensed under a Creative Commons Attribution-NonCommercial 3.0 Unported Licence.

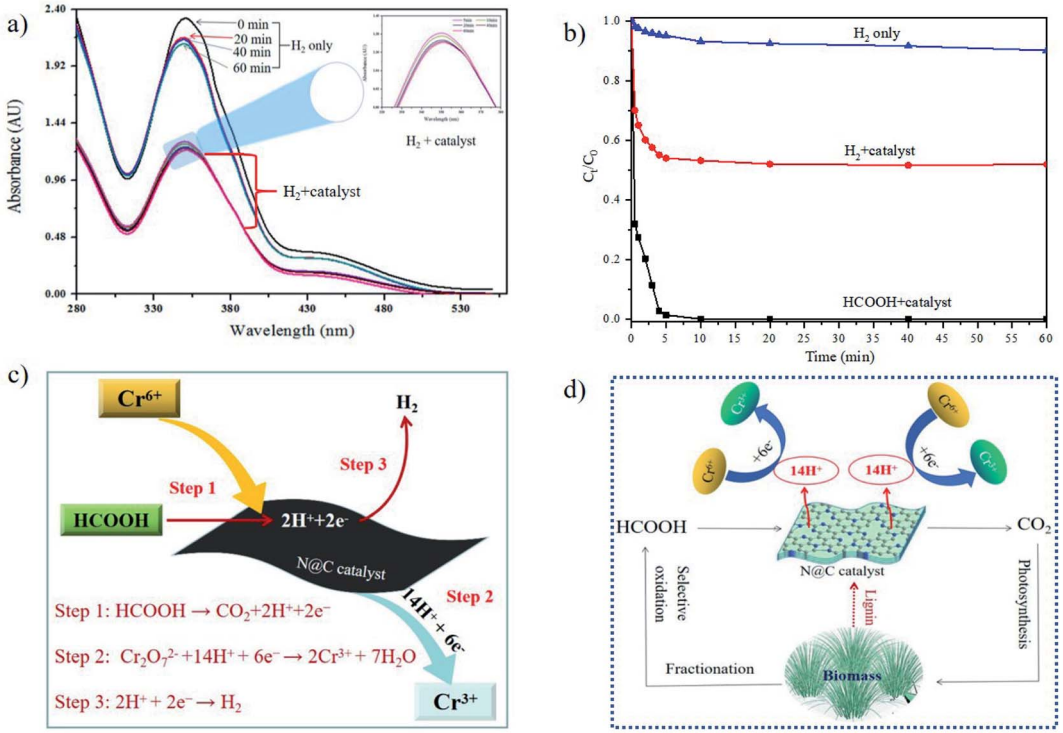

Fig. 6 Presumed catalytic mechanism of HCOOH-mediated reduction of Cr^{6+} by N@C-g-C_3N_4 catalyst. (a) Cr^{6+} reduction using molecular hydrogen as reductant; (b) comparison of catalytic efficiency HCOOH-mediated reduction and molecular hydrogen-mediated reduction of Cr^{6+} by N@C-g-C_3N_4 catalyst; (c) probable catalytic mechanisms of HCOOH-mediated reduction of Cr^{6+} in the presence of N@C-g-C_3N_4 catalyst; (d) the overall reaction of Cr^{6+} reduction over N@C-g-C_3N_4 catalyst *via* HCOOH-mediated transfer hydrogenation. Reaction conditions: 25 mL $K_2Cr_2O_7$ (0.68 mM), 1 mL HCOOH (98%) or H_2 bubble, 25 mg catalyst, room temperature, and stirring rate 500 rpm.

proceeding on catalyst *via* dehydrogenation pathway (HCOOH → CO_2 + $2H^+$ + $2e^-$),[27] following with the reduction of Cr^{6+} to Cr^{3+} through H^+ transfer ($Cr_2O_7^{2-}$ + $14H^+$ + $6e^-$ → $2Cr^{3+}$ + $7H_2O$).[3] Simultaneously, the electrons participate in hydrogen production through H^+ rearrangement ($2H^+$ + $2e^-$ → H_2). The electrons perhaps participate in both hydrogen production and reduction of Cr^{6+} at the same time (Fig. 6c). H_2 released from HCOOH decomposition is monitored by gas chromatography, and CO_2 is confirmed by phenolphthalein coloration, changing from red to colorless in the presence of CO_2 (Fig. S14†). The overall reaction of Cr^{6+} reduction over N@C-g-C_3N_4 catalyst *via* HCOOH-mediated transfer hydrogenation is shown in Fig. 6d. Because HCOOH and lignin are both obtained from biomass. As byproduct of pulp and papermaking, lignin can be cost-effective and easily available. Consequently, the development of processes which can utilize lignins for high value carbon materials has the potential for a high payoff for biomass biorefinery. Therefore, it is undoubted that the proposal strategy of HCOOH-mediated reduction of toxic Cr^{6+} by N@C-g-C_3N_4 is a green and renewable procedure.

3.4 Interferences, stability, and renewability of Cr^{6+} reduction by N@C-g-C_3N_4 catalyst

As well known, wastewater containing Cr^{6+} is usually a mixture of organic and inorganic substances. It is therefore mandatory to investigate the possible interference effect of these interferents on the HCOOH-mediated reduction of Cr^{6+} by N@C-g-C_3N_4 catalyst. The data in Fig. 7a show that a decrease in the catalytic reduction efficiency of Cr^{6+} by N@C-g-C_3N_4 is observed in the presence of 1 mL (0.2 mM) of inorganic ions interferents such as Cl^-, SO_4^{2-}, HPO_4^{2-}, and NO_3^-, the probable reason is the fact that inorganic ions possess stable and maximum oxidation states and cannot hold electrons or holes.[1] However, organic interferents, glucose, citric acid, urea, and sucrose, have no noteworthy effect of Cr^{6+} reduction (Fig. 7b) due to the lack of the competency with Cr^{6+}.[1] N@C-g-C_3N_4 catalyst shows astounding stability with no activity loss even after 8 months storage (Fig. 7c). Furthermore, as shown in Fig. 7d, the catalyst remains operational stability after five recycling usages, revealing a good renewability of N@C-g-C_3N_4. The structural properties of the used catalyst were characterized by TEM, HR-TEM, Raman, and TGA techniques, and it has demonstrated that no variation in the structure is found after five cycles of catalytic reaction (Fig. 7e–g), further confirming the structural stability of N@C-g-C_3N_4.

3.5 Extended hydrogenation reactions and removal of organic dyes

To explore the practical applications of N@C-g-C_3N_4-950, extended experiments were tested on the catalytic activities in other hydrogenation reactions of 4-NP, BPA and $K_3[Fe(CN)_6]$ using $NaBH_4$ as hydrogen donor.[13,28] For hydrogenation of

© 2022 The Author(s). Published by the Royal Society of Chemistry

Open Access Article. Published on 04 February 2022. Downloaded on 5/3/2026 9:12:31 AM.
This article is licensed under a Creative Commons Attribution-NonCommercial 3.0 Unported Licence.

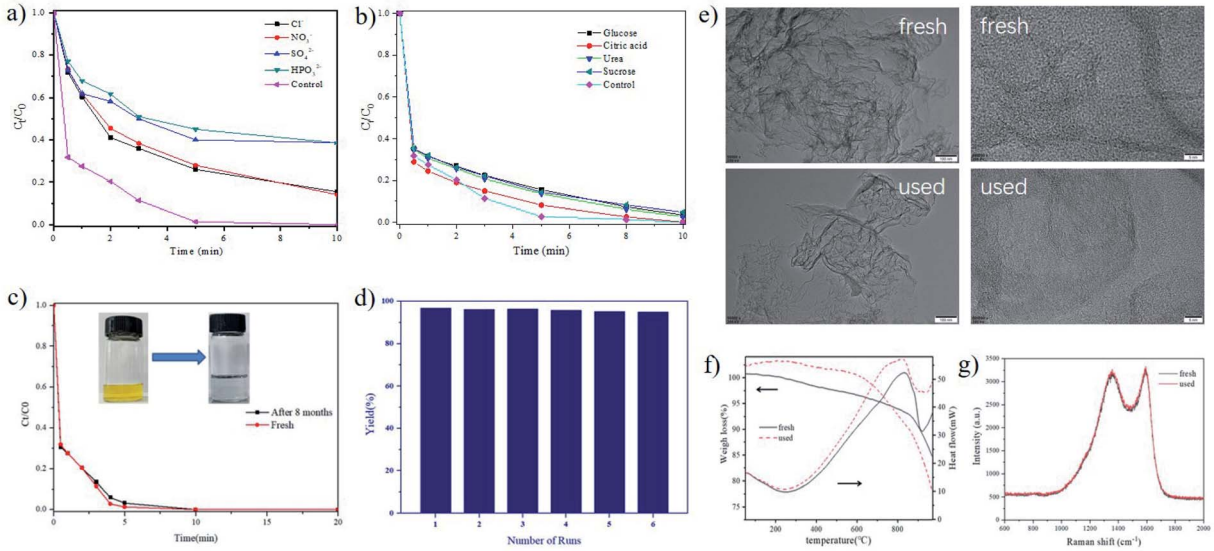

Fig. 7 Interferences, stability, and renewability of N@C-g-C_3N_4-950. (a) Effects of ions; (b) effects of organic compounds; (c) store stability after 8 months; (d) operational stability after 6 cycles; (e) TEM images of fresh and used catalyst; (f) TGA curves of fresh and used catalyst; (g) Raman curves of fresh and used catalyst. Reaction conditions: 25 mL $K_2Cr_2O_7$ (0.68 mM), 1 mL HCOOH (98%), 25 mg catalyst, room temperature, and stirring rate 500 rpm.

nitrogroups, 4-NP can be completely reduced by N@C-g-C_3N_4-950 using $NaBH_4$ as hydrogen donor within 5 min (Fig. S15a†). It has been confirming that 4-NP ions adsorption has an essential influence on catalytic reduction, and the active sites of nitrogen doped carbon for 4-NP reduction are the carbon atoms adjacent to the N dopants.[13] Furthermore, N@C-g-C_3N_4 can also be catalyzed the hydrogenation reaction of $K_3[Fe(CN)_6]$ with $NaBH_4$ as a hydrogen donor. As seen from Fig. S15b,† N@C-g-C_3N_4-950 shows an admirable catalytic activity toward $K_3[Fe(CN)_6]$ reduction. In addition, N@C-g-C_3N_4-950 can also be applied in the reduction of BPA using PMS as hydrogen donor. It is shown that the conversion of BPA increases with reaction time and it is almost completely degraded in 10 min (Fig. S15c†). Owing to its high S_{BET} and mesoporous size, N@C-g-C_3N_4-950 can be conducted to show satisfactory adsorption capacity towards the removal of organic dyes involving methyl red, methyl blue, methylene blue (MB), and congo red (Fig. S15d†). These preliminary research data suggest that N@C-g-C_3N_4-950 shows promising potential practical applications in remediation of contaminated environment.

4 Conclusions

In summary, nitrogen-doped carbon as metal-free catalyst was successfully synthesized through facile calcination in argon atmosphere using lignin as carbon. The as-prepared carbon-based catalyst was characterized by TEM, HR-TEM, Raman, TGA, EDS-mapping, XPS and BET techniques. Among all these catalysts in hand, N@C-g-C_3N_4-950 exhibits the best excellent catalytic capacity with the highest k value of 2.98 min^{-1} and mass specific activity value of 2.21 $mol_{K2Cr2O7}$ g^{-1} min^{-1} in HCOOH-mediated reduction of Cr^{6+} by assessment of activity, interference, stability, and reusability. It is demonstrated that the reduction efficiency of Cr^{6+} to Cr^{3+} was significantly dependent on HCOOH concentration, reaction temperature, pH, catalyst loading, Cr^{6+} concentration. Furthermore, N@C-g-C_3N_4-950 is also proved to be applicable in other hydrogenation reactions involving $K_3[Fe(CN)_6]$, 4-NP and BPA using $NaBH_4$ as reductant, and the removal of organic dyes of methyl red, methyl blue, methylene blue, and congo red, which further researches will be ongoing in our lab. Although the postulated mechanism of HCOOH-mediated dehydrogenation for Cr^{6+} reduction is perhaps the electrons participation in both hydrogen production and reduction of Cr^{6+} at the same time, however, the catalytic mechanism of the reduction of Cr^{6+} to Cr^{3+} by N@C catalyst is still controversial, for example, (1) what are the ideal active sites? (2) what is the role of electron and H^+ species decomposited from HCOOH? These issues will arouse scientists enormous interest in future.

Author contributions

Y. L. completed conceptualization and supervision of this project and drafted the manuscript. H. Y. performed the experiments.

Conflicts of interest

The authors declare no conflicts of interest.

Acknowledgements

This study was funded by The National Key Research and Development Program of China (2021YFC2101304), and the Construction of Innovative Hunan Province of China

(2019NK2031-3) and Hubei University of Science and Technology (2019-20KZ05).

Open Access Article. Published on 04 February 2022. Downloaded on 5/3/2026 9:12:31 AM. This article is licensed under a Creative Commons Attribution-NonCommercial 3.0 Unported Licence.

References

1 B. Vellaichamy, P. Prakash and B. Nagulan, Reduction of Cr^{6+} from wastewater using a novel in situ-synthesized PANI/MnO_2/TiO_2 nanocomposite: renewable, selective, stable, and synergistic catalysis, *ACS Sustainable Chem. Eng.*, 2017, **5**, 9313–9324, DOI: 10.1021/acssuschemeng.7b02324.

2 Y. Gao, C. Chen, X. Tan, H. Xu and K. Zhu, Polyaniline-modified 3D-flower-like molybdenum disulfide composite for efficient adsorption/photocatalytic reduction of Cr(VI), *J. Colloid Interface Sci.*, 2016, **476**, 62–70, DOI: 10.1016/j.jcis.2016.05.022.

3 S. Dai, X. Wu, J. Zhang, Y. Fu and W. Li, Coenzyme A-regulated Pd nanocatalysts for formic acid-mediated reduction of hexavalent chromium, *Chem. Eng. J.*, 2018, **351**, 959–966, DOI: 10.1016/j.cej.2018.06.138.

4 M. Omole, I. Owino and O. Sadik, Palladium nanoparticles for catalytic reduction of Cr(VI) using formic acid, *Appl. Catal., B*, 2007, **76**, 158–167, DOI: 10.1016/j.apcatb.2007.05.018.

5 M. Liang, R. Su, W. Qi, Y. Zhang, R. Huang, Y. Yu, L. Wang and Z. He, Reduction of hexavalent chromium using recyclable Pt/Pd nanoparticles immobilized on procyanidin-grafted eggshell membrane, *Ind. Eng. Chem. Res.*, 2014, **53**, 13635–13643, DOI: 10.1021/ie5021552.

6 M. Celebi, K. Karakas, I. Ertas, M. Kaya and M. Zahmakiran, Palladium nanoparticles decorated graphene oxide: active and reusable nanocatalyst for the catalytic reduction of hexavalent chromium(VI), *ChemistrySelect*, 2017, **2**, 8312–8319, DOI: 10.1002/slct.201700967.

7 F. Shao, J. Feng, X. Lin, L. Jiang and A. Wang, Simple fabrication of AuPd@Pd core-shell nanocrystals for effective catalytic reduction of hexavalent chromium, *Appl. Catal., B*, 2007, **76**, 158–167, DOI: 10.1016/j.apcatb.2017.02.051.

8 T. Xu, J. Xue, X. Zhang, G. He and H. Chen, Ultrafine cobalt nanoparticles supported on reduced graphene oxide: efficient catalyst for fast reduction of hexavalent chromium at room temperature, *Appl. Surf. Sci.*, 2017, **402**, 294–300, DOI: 10.1016/j.apsusc.2017.01.114.

9 K. Bhowmik, A. Mukherjee, M. Mishra and G. De, Stable Ni nanoparticle-reduced graphene oxide composites for the reduction of highly toxic aqueous Cr(VI) at room temperature, *Langmuir*, 2014, **30**, 3209–3216, DOI: 10.1021/la500156e.

10 R. Nie, Y. Tao, Y. Nie, T. Lu, J. Wang, Y. Zhang, X. Lu and C. Xu, Recent advances in catalytic transfer hydrogenation with formic acid over heterogeneous transition metal catalysts, *ACS Catal.*, 2021, **11**, 1071–1095, DOI: 10.1021/acscatal.0c04939.

11 J. Zhang, L. Qu, G. Shi, J. Liu, J. Chen and L. Dai, N,P-codoped carbon networks as efficient metal-free bifunctional catalysts for oxygen reduction and hydrogen evolution reactions, *Angew. Chem., Int. Ed.*, 2016, **55**, 2230–2234, DOI: 10.1002/ange.201510495.

12 G. Wang, Y. Sun, D. Li, H. Liang, R. Dong, X. Feng and K. Millen, Controlled synthesis of N-doped carbon nanospheres with tailored mesopores through self-assembly of colloidal silica, *Angew. Chem.*, 2015, **127**, 15406–15411, DOI: 10.1002/ange.201507735.

13 Y. Liu, H. Xu, H. Yu, H. Yang and T. Chen, Synthesis of lignin-derived nitrogen-doped carbon as a novel catalyst for 4-NP reduction evaluation, *Sci. Rep.*, 2020, **10**, 20075–20088, DOI: 10.1038/s41598-020-76039-9.

14 Y. Zhu, C. Cao, W. Jiang, S. Yang, J. Hu, W. Song and L. Wan, Nitrogen, phosphorus and sulfur co-doped ultrathin carbon nanosheet as a metal-free catalyst for selective oxidation of aromatic alkanes and oxygen reduction reaction, *J. Mater. Chem. A*, 2016, **4**, 18470–18477, DOI: 10.1039/C6TA08335H.

15 H. Wang, Y. Shao, S. Mei, Y. Lu, M. Zhang, J. Sun, K. Matyjaszewski, M. Antonietti and J. Yuan, Polymer-derived heteroatom-doped porous carbon materials, *Chem. Rev.*, 2020, **120**, 9363–9419.

16 H. Zhou, S. Hong, H. Zhang, Y. Chen, H. Xu, X. Wang, Z. Jiang, S. Chen and Y. Liu, Toward biomass-based single-atom catalysts and plastics: highly active single- atom Co on N-doped carbon for oxidative esterification of primary alcohols, *Appl. Catal., B*, 2019, **256**, 117767–117776, DOI: 10.1016/j.apcatb.2019.117767.

17 Y. Yu, H. Xu, H. Yu, L. Hu and Y. Liu, Formic acid fractionation towards highly efficient cellulose-derived PdAg bimetallic catalyst for H_2 evolution, *Green Energy Environ.*, 2022, **7**, 172–183.

18 S. Han, J. Bai, H. Liu, J. Zeng, J. Jiang, Y. Chen and J. Lee, The one-pot fabrication of hollow and porous Pd-Cu alloy nanospheres and their remarkably improved catalytic performance for the hexavalent chromium reduction, *ACS Appl. Mater. Interfaces*, 2016, **8**, 30948–30955, DOI: 10.1021/acsami.6b10343.

19 M. Celebi, K. Karakas, I. Ertas, M. Kaya and M. Zahmakiran, Palladium nanoparticles decorated graphene oxide: active and reusable nanocatalyst for the catalytic reduction of hexavalent chromium(VI), *ChemistrySelect*, 2017, **2**, 8312–8319, DOI: 10.1002/slct.201700967.

20 Y. Huang, H. Ma, S. Wang, M. Shen, R. Guo, X. Cao, M. Zhu and X. Shi, Efficient catalytic reduction of hexavalent chromium using Palladium nanoparticle-immobilized electrospun polymer nanofibers, *ACS Appl. Mater. Interfaces*, 2012, **4**, 3054–3061, DOI: 10.1021/am300417s.

21 L. Wei, R. Gu and J. Lee, Highly efficient reduction of hexavalent chromium on amino-functionalized palladium nanowires, *Appl. Catal., B*, 2015, **176**, 325–330, DOI: 10.1016/j.apcatb.2015.03.056.

22 M. Qamar, M. Gondal and Z. Yamani, Synthesis of nanostructured NiO and its application in laser-induced photocatalytic reduction of Cr(VI) from water, *J. Mol. Catal. A*, 2011, **341**, 83–88, DOI: 10.1016/j.molcata.2011.03.029.

23 S. Gao, W. Liu, C. Feng, N. Shang and C. Wang, Ag-Pd alloy supported on amine-functionalized UiO-66 as an efficient synergetic catalyst for dehydrogenation of formic acid at

 © 2022 The Author(s). Published by the Royal Society of Chemistry

Open Access Article. Published on 04 February 2022. Downloaded on 5/3/2026 9:12:31 AM.
This article is licensed under a Creative Commons Attribution-NonCommercial 3.0 Unported Licence.

room temperature, *Catal. Sci. Technol.*, 2016, **6**, 869–874, DOI: 10.1039/C5CY01190F.

24 S. Li, Y. Ping, J. Yan, H. Wang, M. Wu and Q. Jiang, Facile synthesis of AgAuPd/graphene with high performance for hydrogen generation from formic acid, *J. Mater. Chem. A*, 2015, **3**, 14535–14538, DOI: 10.1039/C5TA03111G.

25 X. Zhang, N. Shang, X. Zhou, C. Feng, S. Gao, Q. Wu, Z. Wang and C. Wang, AgPd-MnOx supported on carbon nanospheres: an efficient catalyst for dehydrogenation of formic acid, *New J. Chem.*, 2017, **41**, 3443–3449, DOI: 10.1039/C6NJ03873E.

26 B. Marinho, R. Cristóvão, R. Djellabi, J. Loureiro, R. Boaventura and V. Vilar, Photocatalytic reduction of Cr(VI) over TiO_2-coated cellulose acetate monolithic structures using solar light, *Appl. Catal., B*, 2017, **203**, 18–30, DOI: 10.1016/j.apcatb.2016.09.061.

27 M. Shao, J. Odell, M. Humbert, T. Yu and Y. Xia, Electrocatalysis on Shape-Controlled Palladium Nanocrystals: Oxygen Reduction Reaction and Formic Acid Oxidation, *J. Phys. Chem. C*, 2013, **117**, 4172–4180, DOI: 10.1021/jp312859x.

28 M. Sajjadi, M. Nasrollahzadeh and M. Tahsili, Catalytic and Antimicrobial Activities of Magnetic Nanoparticles Supported N-Heterocyclic Palladium(II) Complex: A Magnetically Recyclable Catalyst for the Treatment of Environmental Contaminants in Aqueous Media, *Sep. Purif. Technol.*, 2019, **227**, 115716–115726, DOI: 10.1016/j.seppur.2019.115716.